Synthesis and Structure of Polymorph B of Zeolite Beta

Avelino Corma,*[,†] Manuel Moliner,[†] Ángel Cantín,[†] María J. Díaz-Cabañas,[†] José L. Jordá,[†] Daliang Zhang,[‡,§] Junliang Sun,[‡,§] Kjell Jansson,[||,§] Sven Hovmöller,[‡] and Xiaodong Zou*[,‡,§]

Instituto de Tecnología Química, UPV-CSIC, Universidad Politécnica de Valencia, Avenida de los Naranjos s/n, 46022 Valencia, Spain, Structural Chemistry Department, Stockholm University, SE-106 91 Stockholm, Sweden, Inorganic Chemistry Department, Stockholm University, SE-106 91 Stockholm, Sweden, and Berzelii Centre EXSELENT on Porous Materials, Stockholm University, SE-106 91 Stockholm, Sweden

Received January 23, 2008. Revised Manuscript Received March 3, 2008

It was found that either polymorph B or polymorph C of zeolite beta can be obtained from the same structure directing agent: 4,4-dimethyl-4-azonia-tricyclo[5.2.2.$0^{2,6}$]undec-8-ene hydroxide. The synthesis occurs through a consecutive process where polymorph B is first formed and then transformed into polymorph C. It is possible to produce a zeolite highly enriched in polymorph B, provided that the transformation of this phase into polymorph C is slowed down up to the point where polymorph C is only detected at trace levels. The structure of polymorph B was determined for the first time by electron crystallography with SAED and HRTEM from areas of unfaulted polymorph B crystals.

Introduction

Zeolites are crystalline microporous materials that show interesting properties in catalysis, gas separation, and other important technological applications.[1,2] Currently, 179 recognized zeolite framework types[3] have been synthesized within a large spectrum of pore diameters and topology networks.[4–9] The synthesis of a particular structure, when several potential structures compete, is determined by variables such as the silica source, organic structure directing agent (OSDA), presence of other framework elements, gel composition, synthesis temperature, and time. Since the crystallization of a specific material in zeolite synthesis is kinetically controlled, a thermodynamically less stable OSDA−zeolite composite can crystallize in a given system. Nevertheless, the relative stability of potentially competing nuclei toward redissolution may indicate as to which zeolite will preferentially be formed during the early stages of synthesis.[10,11]

Burton has nicely shown, by molecular modeling and experimental work, the important role of an OSDA on the stabilization of a particular structure.[12] However, zeolites are metastable phases, and a sequential phase transformation can occur in structures of the same family that present different thermodynamic stabilities.

The family of zeolite beta consists of three polymorphs:[13–15] polymorph A (***BEA**, $P4_122$, $a = 12.632$ Å and $c = 26.186$ Å), polymorph B ($C2/c$, $a = 17.896$ Å, $b = 17.920$ Å, $c = 14.328$ Å, and $\beta = 114.8°$), and polymorph C (**BEC**, $P4_2/mmc$, $a = 12.769$ Å and $c = 12.977$ Å). The different polymorphs are built from different stacking of the same building layer (Figure 1). While the structure of polymorph C was determined by several different techniques,[16–18] the structures of polymorphs A and B are still hypothetical. Electron crystallography has been shown to be an important technique in structure determination of nanosized crystals

* Corresponding authors. (A.C.) Tel.: 34(96)3877800; fax: 34(96)3877809; e-mail: acorma@itq.upv.es. (X.Z.) E-mail: zou@struc.su.se.
† Instituto de Tecnología Química.
‡ Structural Chemistry Department, Stockholm University.
§ Berzelii Centre EXSELENT on Porous Materials, Stockholm University.
|| Inorganic Chemistry Department, Stockholm University.

(1) Davis, M. E. *Nature (London, U.K.)* **2002**, *417*, 813–821.
(2) Corma, A. *J. Catal.* **2003**, *216*, 298–312.
(3) (a) http://www.iza-structure.org/databases. (b) Baerlocher, C.; Meier, W. M.; Olson, D. H. *Atlas of Zeolite Framework Types*, 5th revised ed.; Elsevier: Amsterdam, 2001.
(4) Strohmaier, K. G.; Vaughan, D. E. *J. Am. Chem. Soc.* **2003**, *125*, 16035–16039.
(5) Burton, A.; Elomari, S.; Chen, C.-Y.; Medrud, R. C.; Chan, I. Y.; Bull, L. M.; Kibby, C.; Harris, T. V.; Zones, S. I.; Vittoratos, E. S. *Chem.—Eur. J.* **2003**, *9*, 5737–5748.
(6) (a) Paillaud, J. L.; Harbuzaru, B.; Patarin, J.; Bats, N. *Science (Washington, DC, U.S.)* **2004**, *304*, 990–992. (b) Corma, A.; Díaz-Cabañas, M. J.; Rey, F.; Nicolopoulus, S.; Boulahya, K. *Chem. Commun. (Cambridge, U.K.)* **2004**, *12*, 1356–1357.
(7) Corma, A.; Rey, F.; Rius, J.; Sabater, M. J.; Valencia, S. *Nature (London, U.K.)* **2004**, *431*, 287–290.
(8) Corma, A.; Diaz-Cabañas, M. J.; Martinez-Triguero, J.; Rey, F.; Rius, J. *Nature (London, U.K.)* **2002**, *418*, 514–517.
(9) Corma, A.; Diaz-Cabañas, M. J.; Jordá, J. L.; Martinez, C.; Moliner, M. *Nature (London, U.K.)* **2006**, *443*, 842–845.
(10) Sastre, G.; Leiva, S.; Sabater, M. J.; Gimenez, I.; Rey, F.; Valencia, S.; Corma, A. *J. Phys. Chem. B* **2003**, *107*, 5432–5440.
(11) Lowe, B. M. *Zeolites* **1983**, *3*, 300–305.
(12) Burton, A. W. *J. Am. Chem. Soc.* **2007**, *129*, 7627–7637.
(13) Newsam, J. M.; Trecy, M. M. J.; Koetsier, W. T.; de Gruyter, C. B. *Proc. R. Soc. London, Ser. A* **1988**, *420*, 375–405.
(14) Treacy, M. M. J.; Newsam, J. M. *Nature (London, U.K.)* **1988**, *332*, 249–251.
(15) Higgins, J. B.; LaPierre, R. B.; Schlenker, J. L.; Rohrman, A. C.; Wood, J. D.; Kerr, G. T.; Rohrbaugh, W. J. *Zeolites* **1988**, *8*, 446–452.
(16) Conradson, T.; Dadachov, M. S.; Zou, X. D. *Microporous Mesoporous Mater.* **2000**, *41*, 183–191.
(17) Corma, A.; Navarro, M. T.; Rey, F.; Rius, J.; Valencia, S. *Angew. Chem., Int. Ed.* **2001**, *40*, 2277–2280.
(18) Liu, Z.; Ohsuna, T.; Terasaki, O.; Camblor, M. A.; Diaz-Cabañas, M.-J.; Hiraga, K. *J. Am. Chem. Soc.* **2001**, *123*, 5370–5371.
(19) Zou, X. D.; Hovmöller, S. *Acta Crystallogr., Sect. A: Found. Crystallogr.* **2008**, *64*, 149–160.

10.1021/cm8002244 CCC: $40.75
Published on Web 04/10/2008

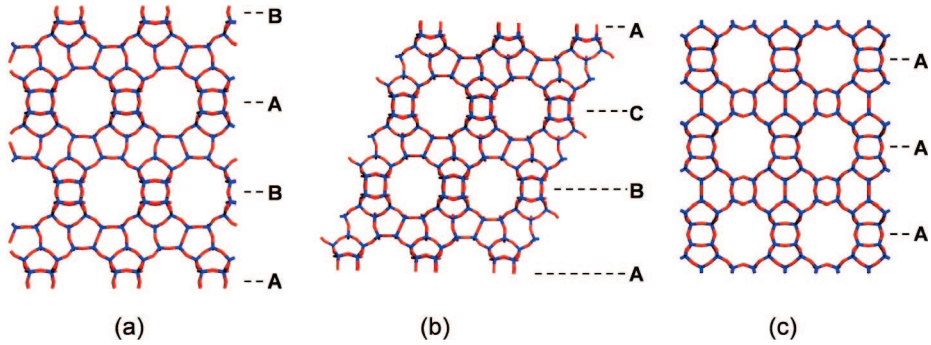

Figure 1. Framework structures of (a) polymorph A, (b) polymorph B, and (c) polymorph C of zeolite beta, showing the different stackings of the 12-ring pores as (a) ABAB. . ., (b) ABCABC. . ., and (c) AA. . ..

including zeolites.[19] There are two main advantages of structure determination by electron crystallography as compared to X-ray diffraction (XRD): (1) crystals millions of times smaller than those needed for X-ray diffraction can be studied and (2) the phases of the crystallographic structure factors, which are lost in XRD, are present in transmission electron microscopy (TEM) images. A combination of electron crystallography with other techniques is even more powerful for the determination of complex structures. One excellent example is the structure determination of the zeolite IM-5 (**IMF**) by combining electron crystallography and the charge-flippy algorithm on powder XRD data.[20]

Recently, a new family of materials enriched in polymorph B of the beta family was reported.[21,22] There, it was claimed that polymorph B/polymorph A ratios were 95:05, 75:25, and 65:35 for NCL-5, NCL-6, and NCL-7, respectively. However, the polymorph ratios were assigned by just comparing the experimental XRD patterns of the samples with the simulated patterns for random intergrowths of polymorphs A and B in those papers, and no crystallographic information was given. A close check of the XRD patterns from the NCL materials (Figures 2 and 3 and of ref 21) shows that a considerable amount of polymorph C of zeolite beta also is present in all NCL samples. The presence of polymorph C easily can be confirmed by a shoulder around the first peak, as well as two separate peaks at 2θ around 22° (Figure 3 of ref 21), one from polymorph B and the other from polymorph C. Taking all these into account, it appears that the results presented do not support the claims by the authors.

Calorimetric experiments[23] indicated that polymorph C of zeolite beta, either as a germanate[16] or silicogermanates,[17] is more stable than zeolite beta, which is an intergrowth of polymorphs A and B (60 and 40%, respectively). Nevertheless, extrapolated values for the pure silica forms indicate that zeolite beta is more stable than polymorph C. However, one should take into account that those values were obtained for samples where the organic molecule was previously removed and that the presence of organic molecules strongly helps to stabilize a given structure during synthesis.

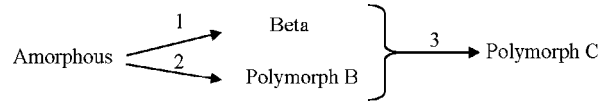

Figure 2. Global crystallization process representing the phase transformation from an amorphous material to beta or polymorph B enriched beta and finally to pure silica polymorph C.

When we carried out the synthesis of the pure silica polymorph C of zeolite beta, it was observed that the formation of polymorph C occurred by a phase transformation from polymorph B enriched beta (Pol A/Pol B = 35:65).[24] Here, we present a synthesis route that maximizes the amount of polymorph B by controlling the reaction kinetics and the raw material sources. A zeolite beta highly enriched with polymorph B (Pol A/Pol B = 15:85) was obtained. Finally, the structure of polymorph B could be determined by electron crystallography from areas of unfaulted polymorph B crystals.

Experimental Procedures

Synthesis and Design of Experiments. The global crystallization process of the zeolite beta family in the presence of 4,4-dimethyl-4-azonia-tricyclo[5.2.2.$0^{2,6}$]undec-8-ene hydroxide (OSDA) can be described by the consecutive transformations of an amorphous material to an intermediate zeolite beta (process 1) or polymorph B (process 2) and then to polymorph C (process 3), as shown in Figure 2. To obtain a material with the highest proportion of polymorph B, process 3 should be minimized. Following this, we explored the variables that influence the crystallization rate, hoping to find conditions where the transformation of polymorph B into polymorph C (process 3) is preferentially slowed down. In addition, it is also necessary that the reaction rate $2 \gg 1$, to produce pure polymorph B or, at least, a material highly enriched in polymorph B.

Since the raw material source is an important synthesis variable and influences the nucleation and growth processes in zeolite synthesis, different silica and titania sources including MCM-41 and Ti-MCM-41 were tested. The Si source and the presence of Ti may have an influence on the kinetics of processes 1 and 2 in the

(20) Baerlocher, C.; Gramm, F.; Massüger, L.; McCusker, L. B.; He, Z. B.; Hovmöller, S.; Zou, X. D. *Science (Washington, DC, U.S.)* **2007**, *315*, 1113–1116.
(21) Kadgaonkar, M. D.; Kasture, M. W.; Bhange, D. S.; Joshi, P. N.; Ramasway, V.; Kumar, R. *Microporous Mesoporous Mater.* **2007**, *101*, 108–114.
(22) Kadgaonkar, M. D.; Kasture, M. W.; Bhange, D. S.; Joshi, P. N.; Ramasway, V.; Gupta, N. M.; Kumar, R. *Microporous Mesoporous Mater.* **2007**, *105*, 82–88.
(23) Li, O.; Navrotsky, A.; Rey, F.; Corma, A. *Microporous Mesoporous Mater.* **2003**, *59*, 177–183.
(24) Cantin, A.; Corma, A.; Díaz-Cabañas, M. J.; Jorda, J. L.; Moliner, M.; Rey, F. *Angew. Chem., Int. Ed.* **2006**, *45*, 8013–8015.

synthesis (Figure 2), thus changing the relative rate of formation and transformation of the intermediate zeolite beta enriched with polymorph B.

MCM-41 and Ti-MCM-41 were synthesized according to a procedure described previously.[25,26] 4,4-Dimethyl-4-azoniatricyclo[5.2.2.0^{2,6}]undec-8-ene hydroxide was used as the SDA. The synthesis of the SDA also was described in previous work.[24] Polymorphs B and C (ITQ-17) of the beta family were synthesized hydrothermally. The synthesis gel was prepared by mixing a silica (or silica/titania) source (Ludox AS-40, MCM-41, or Ti-MCM-41) with alkaline solutions of SDA(OH) and KOH. When Ludox was used as the silica source, titanium(IV) ethoxide was added after the mixture was homogeneous. Finally, an aqueous NH_4F solution was added, resulting in a thick gel. This gel was transferred to a Teflon-lined stainless steel autoclave and heated at 175 °C at different crystallization times. The solids were recovered by filtration, extensively washed with boiling water, and dried at 100 °C overnight. The general gel composition was $SiO_2/xTiO_2/0.5SDAOH/0.25KOH/0.5NH_4F/yH_2O$. Detailed synthesis conditions and final products are given in Table 1.

Characterization Techniques. Powder XRD measurements were performed on a Philips X'Pert MPD diffractometer equipped with a PW3050 goniometer, using Cu $K\alpha_{1,2}$ radiation. The titanium and silicon contents were analyzed with an ICP optical emission spectrometer (Varian 715-ES). Scanning electron microscopy (SEM) was performed on a high-resolution scanning electron microscope (JEOL JSM-7401F) at 2.0 kV with a working distance of 2.0 mm. Solid state ^{19}F NMR spectroscopy was carried out at room temperature on a Bruker AV-400 spectrometer with magic angle spinning (MAS) at 376.28 MHz using a Bruker probe with 2.5 mm diameter zirconia rotors spinning at 25 kHz. Solid state ^{19}F NMR spectra were collected using pulses of 4.5 μs corresponding to a flip angle of $\Pi/2$ rad. A recycle delay of 100 s was used to ensure complete recovery of magnetization.

Structure Determination. Selected area electron diffraction (SAED) and TEM were performed on a JEOL JEM-2000FX instrument at 200 kV with a maximum tilt range of ±45° and on a JEM-3010 instrument at 300 kV with a point resolution of 1.7 Å. Samples for TEM were dispersed in ethanol by ultrasound. A drop of the suspension was transferred onto a copper grid covered by holey carbon films. SAED patterns and high resolution transmission electron microscopy (HRTEM) images were recorded on a KeenView CCD camera from Olympus Soft Imaging Solutions and a Gatan Multiscan 600HP CCD camera, respectively.

Quantification and indexation of SAED patterns were performed by the programs ELD[27] and PhIDO from Calidris, Sweden, respectively. Unit cell parameters were determined from a tilt series of SAED patterns by the program Trice.[28] Amplitudes and phases of the crystallographic structure factors were determined from HRTEM images by the program CRISP.[29] 3-D potential maps were reconstructed using the program eMap from AnaliTEX, from which atomic coordinates of the Si atoms were determined.[30] Atomic

Table 1. Synthesis Conditions for the Studied Samples

	Direct Synthesis[a]							Transformation of Ti-MCM-41[a]						
	$H_2O/Si = 7.5$		$H_2O/Si = 15$		seeding with B(85)		$H_2O/Si = 20$		$H_2O/Si = 7.5$			$H_2O/Si = 15$		
TiO_2/SiO_2	7 days	14 days	7 days	14 days	7 days	14 days	14 days	TiO_2/SiO_2	7 days	14 days	30 days	7 days	14 days	30 days
without Ti	C−B(60)	C	B(85)	C−B(85)	B(85)	B(85)−C	amorphous	without Ti	B(50)	C	C	B(55)	B(55)	B(55)−C
1 wt %	C−B(60)	C	B(75)−amorphous	B(75)				1 wt %				B(65)−amorphous	B(65)	B(65)−C
2 wt %	B(60)−C	B(60)−C	amorphous	B(65)				2 wt %	B(50)	B(50)−C	C	B(85)−amorphous	B(85)	B(85)−C
								3 wt %				amorphous	amorphous	amorphous
4 wt %	B(60)	B(60)−C	amorphous	amorphous−B(60)				4 wt %				amorphous	amorphous	amorphous

[a] Phase B is the intergrowth of polymorphs A/B with the ratio of B inside the parentheses, determined from XRD. Phase C is the polymorph C of zeolite beta.

(25) Corma, A.; Domine, M.; Gaona, J. A.; Jorda, J. L.; Navarro, M. T.; Rey, F.; Perez-Pariente, J.; Tsuji, J.; McCullock, B.; Nemeth, L. T. *Chem. Commun. (Cambridge, U.K.)* **1998**, *20*, 2211–2212.
(26) Blasco, T.; Corma, A.; Navarro, M. T.; Perez-Pariente, J. *J. Catal.* **1995**, *156*, 65–74.
(27) Zou, X. D.; Sukharev, Y.; Hovmöller, S. *Ultramicroscopy* **1993**, *49*, 147–158.
(28) Zou, X. D.; Hovmöller, A.; Hovmöller, S. *Ultramicroscopy* **2004**, *98*, 187–193.
(29) Hovmöller, S. *Ultramicroscopy* **1992**, *41*, 121–135.
(30) Oleynikov, P. http://www.analitex.com.

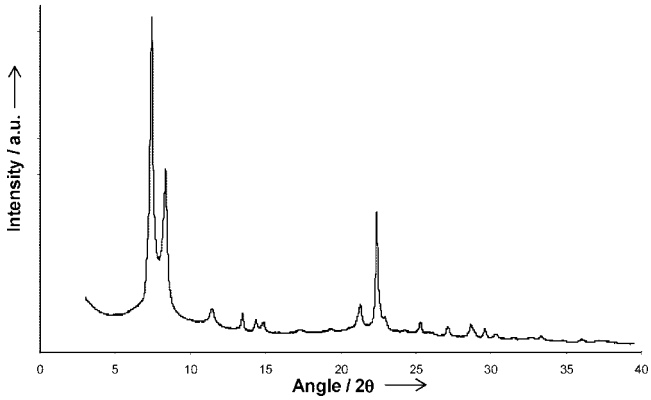

Figure 3. Powder XRD pattern of zeolite beta mostly enriched in polymorph B.

coordinates of Si and O atoms were refined by distance least-squares refinement using the program DLS-76.[31]

Results and Discussion

Synthesis of Polymorph B of Beta Family. We found that the H_2O/SiO_2 ratio is important for controlling the transformation rate of beta or polymoph B to polymorph C. At a H_2O/SiO_2 ratio of 7.5, an amorphous material first was formed that evolved into a beta-type zeolite enriched in polymorph B (60%) after 7 days (Table 1). This was transformed into polymorph C, and the pure silica polymorph C was synthesized in 14 days. To decrease the rate of this transformation, we increased the dilution of the gel to $H_2O/SiO_2 = 15$. Since all the beta samples obtained present a higher content in polymorph B than usual, it seems that this SDA favors, preferentially, the formation of polymorph B instead of A. Because of that, increasing the gel dilution should also favor the formation of the thermodynamically more stable phase, polymorph B. Indeed, at $H_2O/SiO_2 = 15$, a material with 85 ± 5% of polymorph B and 15 ± 5% of polymorph A was obtained (see Table 1 and Figure 3). This was determined by comparing the XRD pattern of the experimental sample with simulated diffraction patterns of zeolite beta containing different A/B ratios, obtained with the DIFFaX program[32] (see Figure 4).

In the sample with the highest ratio of polymorph B, the presence of polymorph C could not be detected by XRD. However, the ^{19}F MAS NMR spectrum of the as-made material has three signals at −38.3, −60.7, and −70.3 ppm (Figure 5). The very small signal at −38.3 ppm is assigned to the presence of fluoride anions within double 4-ring (D4R) units.[33] These secondary building units are present neither in polymorph A nor in B but only in polymorph C. Therefore, even if polymorph C cannot be detected by XRD, we can say that it is present in the material at trace levels.

When the synthesis at $H_2O/SiO_2 = 15$ was prolonged for 14 days, some of the material enriched with polymorph B still was present, although polymorph C was the major phase observed. A further gel dilution ($H_2O/SiO_2 = 20$) strongly slowed down the rate of crystallization, and even after 14 days, only amorphous material was detected.

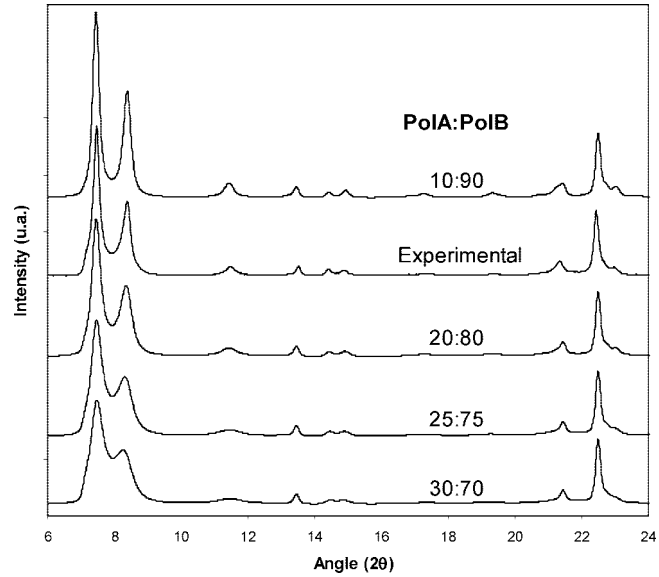

Figure 4. Simulation using the DIFFaX program of the diffraction patterns of zeolite beta with different ratios of polymorphs A/B, indicating that the material is formed by an intergrowth ratio (A/B) of 15:85.

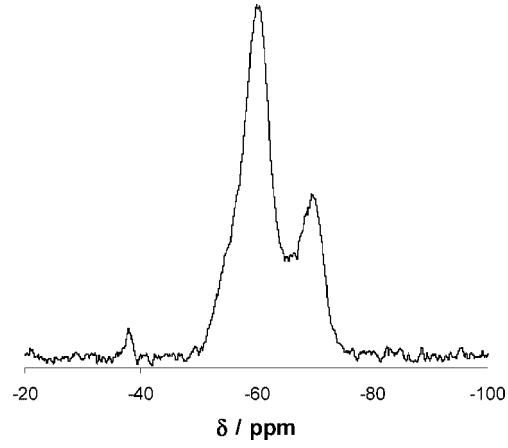

Figure 5. ^{19}F MAS NMR spectrum of the as-made zeolite beta enriched in polymorph B.

Since we achieved a beta sample highly enriched in polymorph B and practically free of polymorph C, we used that material as seed under best synthesis conditions with the aim of favoring the formation of polymorph B. Unfortunately, the results did not improve: 85 ± 5% polymorph B containing material was formed after 7 days. Since the presence of Ti has been reported to decrease the crystallization rate of zeolites,[34] we used different levels of Ti, as Ti(IV) ethoxide, within the synthesis gel. Ti decreases the rate of crystallization of all the different polymorphs but did not increase the polymorph B content (see Table 1).

Finally, silica MCM-41 and Ti containing MCM-41 were used as sources of silica for the synthesis (see Table 1). The rate of crystallization decreased. Only with Ti-MCM-41 (2 wt % Ti) was a sample with 85 ± 5% polymorph B obtained.

(31) Baerlocher, C.; Hepp, A.; Meier, W. M. *DLS-76: Distance Least-Squares Refinement Program*; ETH: Zurich, 1976.
(32) Treacy, M. M. J.; Deem, M. W.; Newsam, J. M. DIFFaX: A Computer Program for Calculating Diffraction from Faulted Crystals. http://www.public.asu.edu/~mtreacy/DIFFaX.html.
(33) Caullet, P.; Guth, J. L.; Hazm, J.; Lamblin, J. M.; Gies, H. *Eur. J. Solid State Inorg. Chem.* **1991**, *28*, 345–361.
(34) Reddy, J. S.; Kumar, R. *Zeolites* **1992**, *12*, 95–100.

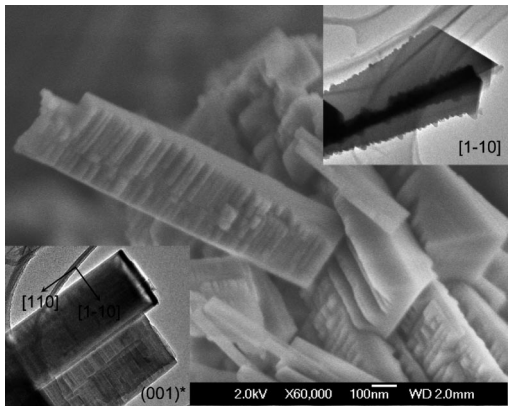

Figure 6. SEM image showing the morphology of polymorph B crystals. Insets are TEM images showing that the crystals are wedge-shaped in the [1–10] projection (top right) and rectangular in the *ab* plane projection (bottom left).

The pure silica sample containing 85% polymorph B was used to determine the crystal structure of polymorph B.

Determination of Polymorph B Structure. The polymorph B enriched sample was studied by both SEM and TEM. The crystals were rod-like with the longest dimension (0.5 to ~2 μm) along the [110] direction and the other two dimensions along the [1–10] direction and that perpendicular to the *ab* plane (0.1 to ~0.7 μm) (see Figure 6). As noted already by Newsam et al.,[13] the crystal surfaces were not smooth. A large number of sharp ridges were formed, as is evident in the SEM image (Figure 6). The crystals are slightly wedge-shaped.

SAED patterns from different areas and different directions show that most crystallites contain twins of polymorph B indicated by twinned SAED patterns or stacking faults indicated by streaks in the SAED patterns. In general, the twinning and stacking faults were observed more frequently near the surface than in the bulk of the crystallites. The unfaulted polymorph B crystals are large enough for a complete structure determination of polymorph B by electron crystallography on SAED and HRTEM. The structure solution is presented next.

The unit cell of polymorph B was determined from a tilt series of SAED patterns, using the programs ELD[27] and Trice.[28] The unit cell parameters were $a = 17.97$ Å, $b = 17.97$ Å, $c = 14.82$ Å, $\alpha = 90°$, $\beta = 113.7°$, and $\gamma = 90°$. The possible space groups were *Cc* and *C*2/*c*, deduced from the reflection conditions observed from the SAED patterns: *hkl*: $h + k = 2n$; *h*0*l*: $h = 2n$ and $l = 2n$; and 0*k*0: $k = 2n$.

HRTEM images of polymorph B taken along the [1–10] direction show clearly 12-ring channels arranged in an ABCABC. . . stacking sequence, characteristic of the polymorph B structure (Figure 7a). The lattice averaged projection derived from the HRTEM images shows two-fold symmetry and is consistent with the space group *C*2/*c* (Figure 7a). Well-resolved 4-, 5-, and 6-ring structures are observed from the HRTEM images.

Structure determination was made from the thinnest area of the polymorph B crystal in the HRTEM image (Figure 7a). Because of the symmetry, HRTEM images taken along the [1–10] direction were equivalent to those taken along the [110] direction. These directions are 90° from each other.

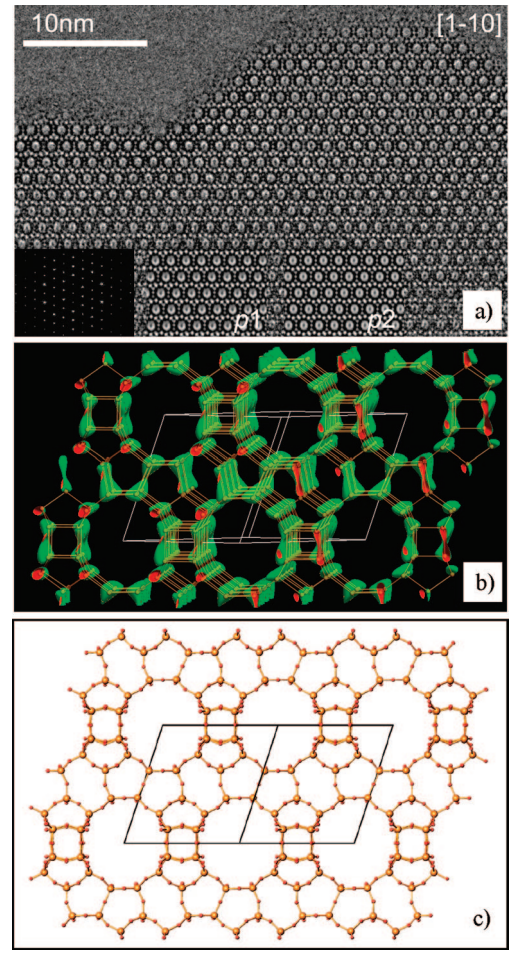

Figure 7. (a) HRTEM image along the [1–10] direction used for structure determination. Except for one row on the top left of the crystal, the crystal along the projection is perfect. Only the area without any defects was used for structure determination. Insets are (from left to right) Fourier transform of this area and average images with *p*1 and *p*2 symmetries. (b) 3-D potential map reconstructed from this HRTEM image. All nine unique Si atoms were found,- and their atomic coordinates were determined from this 3D map. (c) Structure model of polymorph B after distance least-squares refinement. Si atoms are yellow, and O atoms are red.

Thus, it is possible to obtain a complete 3-D structure of polymorph B from the single [1–10] projection. Amplitudes and phases of the crystallographic structure factors of 39 independent reflections with $d > 2.5$ Å were extracted from the [1–10] HRTEM images by the program CRISP.[29] These 39 independent reflections (with indices (*hhl*)) further generated a total of 152 reflections (with indices (*hhl*), ($h-hl$), ($-hh-l$), and ($-h-h-l$)) that were used for reconstructing the 3-D potential map by the program eMap[30] (Figure 7b). All nine Si atoms could be resolved in the 3-D potential map (Table 2). Each of them was connected to four other Si atoms, resulting in a 3-D framework (Figure 7b).

Oxygen atoms could not be resolved at the current resolution of the HRTEM images but were inserted geometrically between the neighboring Si atoms. The nine unique Si and a total of 16 unique O positions were then refined by a distance least-squares refinement using the program DLS-76.[31] The unit cell parameters also were refined by DLS-76 to be $a = 17.70$ (15) Å, $b = 17.70$ (15) Å, $c = 14.33$ (11) Å, and $\beta = 114.89$ (1)°. The final structure

Table 2. Fractional Atomic Coordinates of Si Obtained from the 3-D Potential Map Reconstructed from an HRTEM Image Taken along the [1–10] Direction

atom	x_{EM}[a]	y_{EM}[a]	z_{EM}[a]	deviation (Å)[b]
Si1	0.62	0.97	0.41	0.41
Si2	0.49	0.84	0.41	0.46
Si3	0.69	0.69	0.60	0.42
Si4	0.83	0.84	0.61	0.11
Si5	0.57	0.82	0.61	0.31
Si6	0.71	0.95	0.61	0.15
Si7	0.50	0.88	0.75	0.17
Si8	0.69	0.90	0.24	0.32
Si9	0.50	0.70	0.25	0.43

[a] Standard deviations for coordinates were estimated to be 0.01. [b] Deviations were calculated by comparing atomic positions with those refined by DLS-76.

model of polymorph B (Figure 7c and Table 3) agrees with those proposed in the literature.[3,13–15]

The polymorph B structure was built from a building layer consisting of 12-ring structures. Adjacent layers are related by an inversion center located between the layers. The 12-ring pores are shifted from each other and packed in an ABCABC. . . stacking sequence. The structure of polymorph B contains intersecting channels in three directions, with straight 12-ring channels along the [110] and [1–10] directions and inclined 12-ring channels along the [001] direction.

Conclusion

We found that the same OSDA that directs the formation of polymorph C of zeolite beta can selectively form, in a preceding synthesis step, zeolite beta samples enriched in polymorph B. By optimizing the synthesis conditions, it was possible to obtain zeolite beta highly enriched in polymorph B, provided that the transformation of this phase into polymorph C was slowed down, up to the point where polymorph C was only detected at trace levels. SAED patterns from different areas and directions showed that most crystallites contain twins of polymorph B or stacking faults. The twinning and stacking faults were observed more frequently near the surface than in the bulk of the crystallites. The structure of polymorph B was successfully determined by SAED and HRTEM from the areas of unfaulted polymorph B crystals.

Table 3. Fractional Atomic Coordinates (with esd) of Polymorph B Refined by DLS-76

atom	*x*	*y*	*z*
Si1	0.606(3)	0.979(3)	0.381(4)
Si2	0.482(2)	0.857(3)	0.377(3)
Si3	0.699(3)	0.711(2)	0.606(4)
Si4	0.826(2)	0.834(2)	0.613(3)
Si5	0.580(3)	0.834(3)	0.610(4)
Si6	0.704(3)	0.957(2)	0.615(4)
Si7	0.5	0.889(4)	0.75
Si8	0.695(3)	0.916(2)	0.254(5)
Si9	0.5	0.724(4)	0.25
O1	0.533(4)	0.919(4)	0.348(5)
O2	0.650(4)	0.988(4)	0.503(4)
O3	0.571(3)	1.060(3)	0.332(4)
O4	0.674(4)	0.954(4)	0.341(6)
O5	0.512(4)	0.854(4)	0.499(4)
O6	0.385(3)	0.875(5)	0.327(7)
O7	0.496(6)	0.775(4)	0.339(3)
O8	0.773(4)	0.768(3)	0.629(5)
O9	0.622(4)	0.753(3)	0.612(7)
O10	0.732(4)	0.646(3)	0.692(6)
O11	0.670(4)	0.673(3)	0.496(5)
O12	0.786(3)	0.915(3)	0.620(5)
O13	0.919(2)	0.829(4)	0.702(5)
O14	0.652(4)	0.896(3)	0.646(5)
O15	0.539(4)	0.836(3)	0.691(5)
O16	0.728(4)	1.024(3)	0.697(6)

Acknowledgment. Financial support from the Spanish Government (Project MAT2006-14274-C02–01) and the EU Commission (TOPCOMBI Project) is gratefully acknowledged. M.M. thanks CSIC for an I3P grant. J.S. is supported by a postdoctoral grant from the Carl Trygger Foundation. The Berzelii Centre EXSELENT is supported by the Swedish Research Council (VR) and the Swedish Governmental Agency for Innovation Systems (VINNOVA).

CM8002244